Northumbria Research Link

Northumbria University
NEWCASTLE

UniversityLibrary

Self-toughening and Interfacial Welding of Covalent Adaptable Networks Undergoing Hydro-chemo-mechanical Coupling

Jing Zhang,[†] Xiaojuan Shi,[†] Haibao Lu,[*, †] Kai Yu,[*, ‡] and Yong-Qing Fu[*, §]

[†]National Key Laboratory of Science and Technology on Advanced Composites in Special Environments, Harbin Institute of Technology, Harbin, 150080, PR China

[‡]Department of Mechanical Engineering, University of Colorado Denver, Denver, CO 80217, USA

[§]Faculty of Engineering and Environment, University of Northumbria, Newcastle upon Tyne, NE1 8ST, UK

[*]**Corresponding Authors:** Email: luhb@hit.edu.cn (H.L.), kai.2.yu@ucdenver.edu (K.Y.) and richard.fu@northumbria.ac.uk (Y.F.)

ABSTRACT: Thermosetting epoxy polymers can be designed with recycling, remodeling, and repairing properties owing to the special bond exchange reactions (BERs) in their covalent adaptable networks (CANs). However, the mechanisms behind their complex coupling of hydrodynamic diffusion, molecular reactions, and topological network structure changes have not been fully understood. In this paper, a hydro-chemo-mechanical coupling model is developed to describe self-toughening mechanisms of thermosetting epoxy polymers, wherein the CANs cooperatively undergo the combined processes of hydrodynamic diffusion, chemical BERs, and mechanical topology entanglements. Based on free volume theory and rubber elasticity theory, an extended phantom network model is developed to investigate the synergistic effects of hydrodynamics, BERs, and mechanical topology on interfacial

welding and self-toughening behaviors of the CANs. A constitutive stress-strain relationship is further developed to understand the self-toughening mechanisms of CANs undergoing the hydro-chemo-mechanical coupling. Finally, effectiveness of the proposed model is verified using the results obtained from the experiments and finite element analysis.

1. INTRODUCTION

Covalent adaptable networks (CANs) enable thermosetting polymers to exhibit multiple capabilities of malleability,[1] self-healing,[2-4] reprocessing, and recycling,[5,6] by utilizing bond exchange reactions (BERs) under external stimuli, including heat and light.[1-6] Various covalent bonds have been employed to trigger reversible BERs and molecular rearrangements, including nitroxides,[7-9] acyl hydrazone bonds,[10] disulfide-bonds,[11-13] hemiaminal linkages[14] and transesterification reactions.[15] These BERs provide the thermosetting polymers with interfacial welding and self-healing capabilities, thus significantly extending their practical applications in aerospace,[16-18] manufacturing industry[19] and soft robotics.[20] Here, self-healing of a polymer is defined as the recovery process after its mechanical damage, including the accompanying chemical reconnection of polymer networks. Interfacial welding is defined as the self-healing behavior which occurs at the interface of CANs.

Epoxy polymers are one of the most commonly used materials for high-performance engineering applications.[21-23] However, most of them are chemically crosslinked and can not be easily recycled using conventional techniques, leading to severe environmental pollution and resource wastage.[24,25] CANs have recently been

incorporated into the thermosetting epoxy polymers to achieve their self-healing and recycling capabilities using BERs,[26] and form new generations of green materials, which can be fully recycled and reprocessed without causing environmental pollution.[27]

The interfacial welding behaviors of epoxy polymers have been widely investigated previously.[28-31] For example, Yu et al. studied the welding of the epoxy polymer, which showed recoverable mechanical strength by applying a pressure of 40 kPa at 140°C.[27,32] Their results also revealed that the welding strength of the epoxy polymer became quite poor at a temperature of 22°C and atmospheric pressure due to the high residual stress in the epoxy polymer. Shi et al. developed swelling-assisted interfacial welding approach for epoxy polymers by using the solvent at 100°C.[33] However, self-toughening occurring at room temperature has never been reported so far, and the mechanical strength of interfacial welding is often below 80% of the original strength.[32,33] As will be introduced in detail in the following section, the self-toughening refers to the enhancement in the mechanical properties of epoxy, in which the CANs cooperatively undergo combined processes of hydrodynamic diffusion, chemical BERs, and mechanical topology entanglements. At the interface, BER gives additional mechanical entanglement, of which the topology rearrangement is able to change the microscale network structures and serves as additional crosslinking sites to enhance the stiffness. Therefore, further studies should be thoroughly carried out to fully understand the working mechanisms and optimize the processing conditions of epoxy polymers to enhance their interfacial welding and self-toughening capabilities.

Based on the free volume theory[34] and rubber elasticity theory,[28,35] this study proposes a free-energy equation to understand the cooperatively hydrodynamic BERs[36] and topology entanglements[37-40] of CANs in thermosetting epoxy polymers. Furthermore, an extended phantom network model is formulated to investigate the synergistic effects of diffusion, BERs, and mechanical topology on interfacial welding and self-toughening behaviors associated with the CANs. A constitutive stress-strain relationship is further developed to understand the self-toughening mechanism of epoxy polymers undergoing hydro-chemo-mechanical coupling. Effects of diffusion coefficient, free volume, catalyst concentration, welding time, and activation energy on functional degrees of CANs have been investigated and discussed. Finally, the effectiveness of the proposed model is verified using the results from both the experiments and finite element analysis (FEA).

2. EXPERIMENTAL DETAILS

2.1 Material

The epoxy polymers were synthesized using diglycidyl-ether bisphenol A (DGEBA) as the epoxy monomer and glutaric anhydride as the cross-linker. The stoichiometric ratio between the epoxy and glutaric anhydride was 1 : 0.5. Crosslinking agent was initially mixed with the DGEBA in a beaker and stirred at 80°C for 45 min. Then the mixture was poured into a mold and cured in the oven at 160°C for 24 h. Figure 1(a) shows the reaction between the DGEBA and glutaric anhydride. The synthesized network contains ester bonds on the chain backbone, which can participate in transesterification of BERs with the solvent molecules during

the self-healing process. The DGEBA monomer opens both sides of its loop structure

and is polymerized by the crosslinker to form a chain. Figure 1(b) shows that a CAN

has a crosslinking point linked with three chains. Figure 1(c) presents a hexagonal

structure of the CAN.
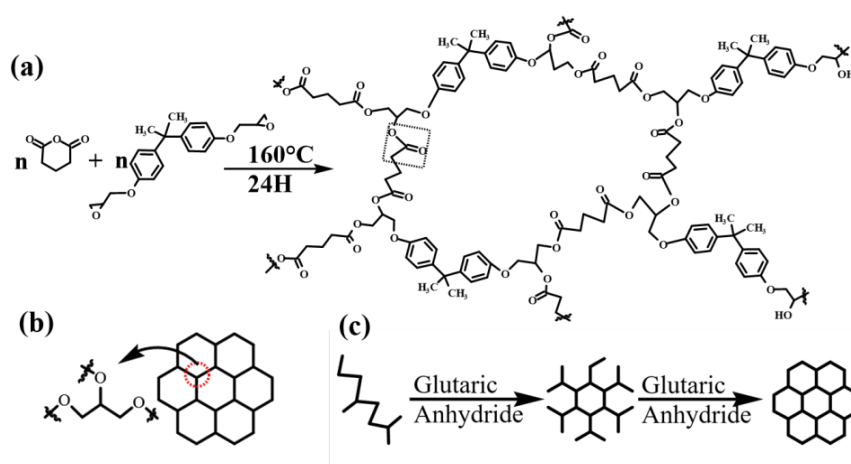
Figure 1. (a) Schematic diagram of the transesterification reactions and BERs in CANs. (b) Schematic diagram of the functional degree of 3 in CANs. (c) Schematic diagram of the effect of glutaric anhydride on CANs.

2.2 Mechanical tests

Mechanical tests were conducted using an electronic universal stretching machine

(AGXplus, Shimadzu, Japan) based on the GB/T1040.2 standard. Figure 2(a) shows

the dimensions of the prepared sample. Figure 2(b) presents the interfacial welding

process of the tested sample after fracture. Schematic illustrations of breaking,

welding, and self-toughening in CANs are illustrated in Figure 2(c). There are three

steps in the interfacial welding process. (1) Curing of CANs from a mixture of

DGEBA and crosslinker to form the epoxy polymer, which is broken owing to the

externally applied stress. (2) Solvent-assisted interfacial welding of CANs via BER.

(3) Topology entanglement of CANs via BER. Here the topology entanglement

process is slightly different from the commonly reported interfacial welding approach, which is the main reason why it can result in the self-toughening of CANs.

Lap-shear tests were adopted to examine the shear bonding strength of welded epoxy samples. According to the GB/T33334 standard, the strain rate was 0.14 min^{-1} at the room temperature of 22°C. The tested sample was firstly cut into two parts with a dimension of 100×25×2 mm^3, and then soaked in 60°C tetrahydrofuran (THF) solution containing 1% 1,5,7-triazabicyclo[4.4.0]dec-5-ene (TBD) catalyst for 45 min. After taken out, the chemical residuals on the sample surface were cleaned, and two cut samples with an overlapping interface of 12.5×25 mm^2 were pressed together at room temperature according to the lap-shear test standard. They were clamped for the interfacial welding and cured in the oven for 45 min. The clips were used to enable a full interfacial welding process.
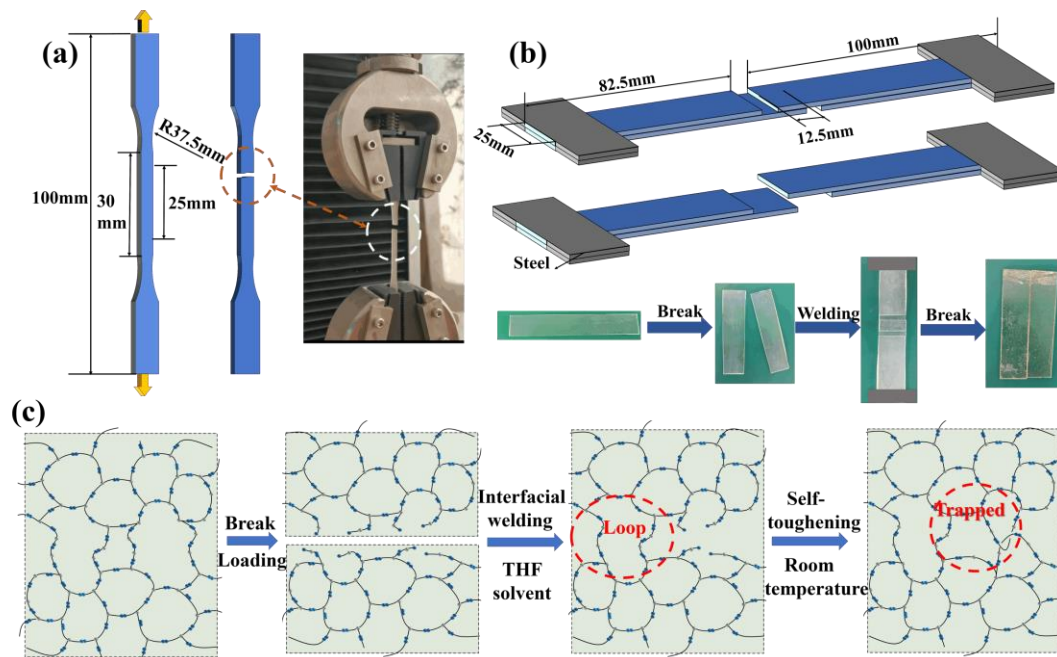
Figure 2. Mechanical measurement and interfacial welding of the tested sample. (a) Tensile test. (b) Interfacial welding. (c) Schematic diagram of break, self-healing, and self-toughening in CANs.

According to the phantom network theory,[41] elastic free energy (ΔF_{el}) of the CANs is expressed as follows:

$$\Delta F_{el} = \left(\frac{1}{2} - \frac{1}{\phi}\right) N k_B T \left(\lambda^2 + 2/\lambda - 3\right) \tag{1}$$

$$\sigma_{xx} = \frac{\partial \Delta F_{el}}{\partial \lambda} = \left(1 - \frac{2}{\phi}\right) N k_B T \left(\lambda - \frac{1}{\lambda^2}\right) = \frac{E}{3}\left(\lambda - \frac{1}{\lambda^2}\right) \tag{2}$$

where $\phi=3$ is the functional degree in the phantom network, as revealed in Figure 1(b). $E=Nk_BT$ is the Young's modulus, λ is the elongation ratio, N is the number of cross-linker, k_B the Boltzmann's constant and σ_{xx} is the stress in uniaxial tension.

Figure 3(a) presents the mechanical properties of the anhydride-cured epoxy polymer, of which the stress-elongation ratio curves were obtained from uniaxial tensile tests and the Young's modulus was obtained as 1.13 GPa. Based on the phantom network theory, the analytical results obtained using the proposed equation (2) have been plotted and compared with the experimental ones as shown in Figure 3(b). These analytical results fit well with the experimental data, where the analytical results show that the Young's modulus is 1.07 GPa with an error $|\Delta E| \leq 0.06$ GPa.
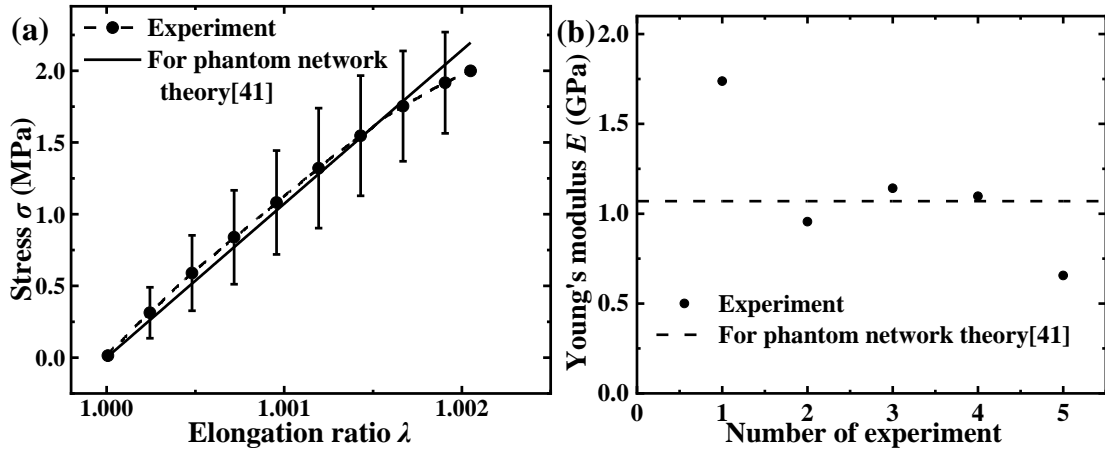
Figure 3. Mechanical properties of anhydride-cured epoxy polymer. (a) The stress-elongation ratio curves. (b) Divergences of analytical and experimental results of Young's moduli.

3. THEORETICAL FRAMEWORK OF INTERFACIAL WELDING

3.1 Diffusion coefficient vs. free volume

Interfacial welding[42-44] is triggered by the catalyst solvent, which diffuses into the CANs to promote the BERs.[45,46] The Fick's second law was used to describe the diffusion of solvent molecules into polymer networks:[33,47,48]

$$\frac{\partial C_0}{\partial t} = D \frac{\partial^2 C_0}{\partial x^2} \tag{3}$$

where C_0 is the mole content of molecule, D is the diffusion coefficient, t is the diffusion time, and x is distance for diffusion.

The diffusion coefficient (D) is determined by the activation energy in an Arrhenius equation,[33]

$$D = D_0 \exp\left(-\frac{E_{as}}{RT}\right) \tag{4}$$

where D_0 is the referenced diffusion coefficient, E_{as} is the diffusion activation energy with a threshold value of 26.8 kJ/mol,[33] R=8.314 J/mol·K is the gas constant, and T is the Kelvin temperature.

Combined with the free volume theory,[41,49] the connection of diffusion coefficient (D_{coop}) to free volume is expressed as,

$$D_{coop} = D_{0c} \exp\left(-\frac{E_{as}}{RT} - \gamma \frac{V_0}{V - k_{so}\Delta Vt - V_0}\right) \tag{5a}$$

$$\Delta m = \rho \cdot \Delta V \tag{5b}$$

where γ=0.5~1 is a given constant, V_0 is the initial volume, V is the final volume after diffusion of solvent molecules, k_{so} represents the volatilization coefficient, ΔV is the change in volume, t is the diffusion time, and ρ=0.89 g/cm^3 is the density of THF.
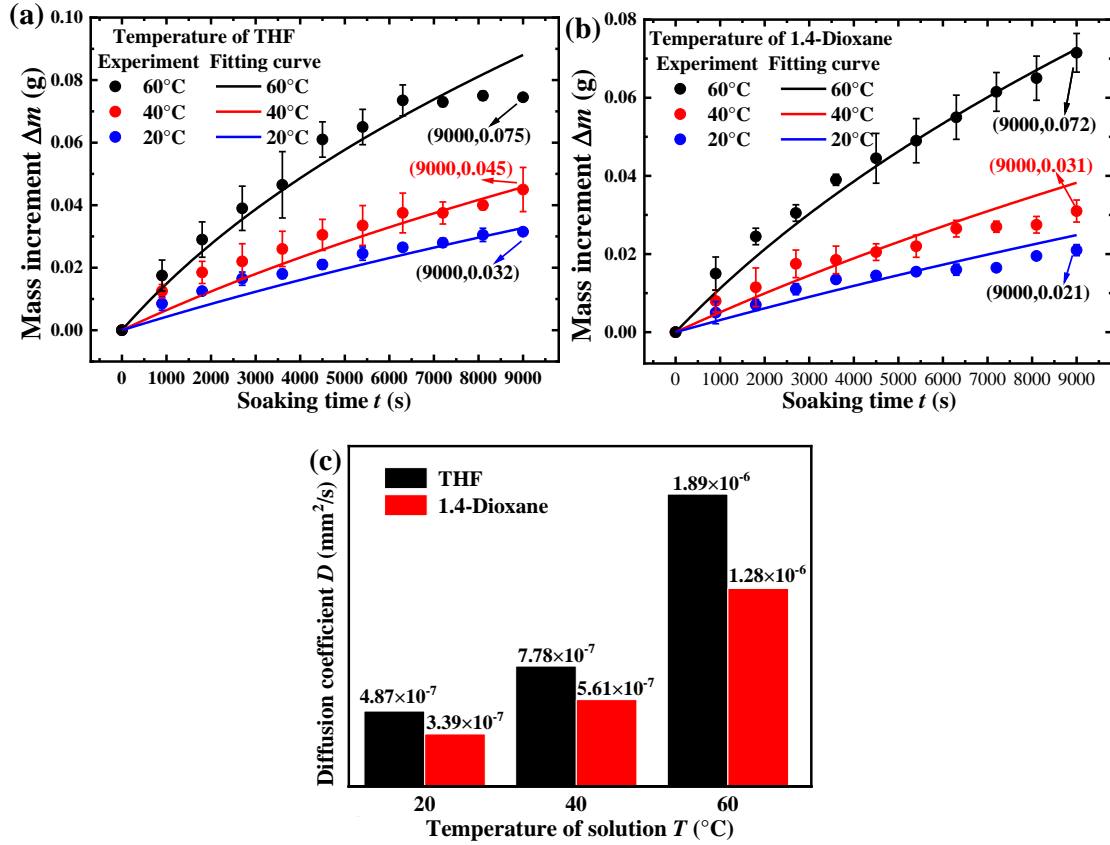
Figure 4. Diffusion behaviors of THF and 1.4-dioxane solvents in the epoxy polymer. (a) Mass increment of epoxy polymer in THF solvent as a function of soaking time. (b) Mass increment of epoxy polymer in 1.4-dioxane solvent as a function of soaking time. (c) Comparison of diffusion coefficients of THF and 1.4-dioxane solvents in the epoxy polymer.

Figure 4 shows the mass increments of the epoxy polymer, in which the solvent molecules have been diffused into the CANs. With an increase in temperature, both the analytical and experimental results reveal that the swelling ratio is increased. With an increase in the temperature of THF solution, the diffusion coefficients (D) at the temperatures of 20°C, 40°C, and 60°C are 4.87×10^{-7} mm^2/s, 7.78×10^{-7} mm^2/s, and 1.89×10^{-6} mm^2/s, respectively, resulting in the increased mass from 0.032 g, 0.045 g to 0.075 g, as shown in Figure 4(a). With the increase of temperature in the 1.4-dioxane solution, the diffusion coefficients (D) at 20°C, 40°C, and 60°C are 3.39×10^{-7} mm^2/s, 5.61×10^{-7} mm^2/s, and 1.28×10^{-6} mm^2/s, respectively, resulting in the increased

mass from 0.021 g, 0.031 g to 0.072 g, as shown in Figure 4(b). A comparison of the diffusion coefficients between the THF and 1.4-dioxane solutions has been presented in Figure 4(c), which reveals that the THF solution enables a high diffusion coefficient of catalyst into the CANs for the BERs.

3.2 Theoretical framework of interfacial welding
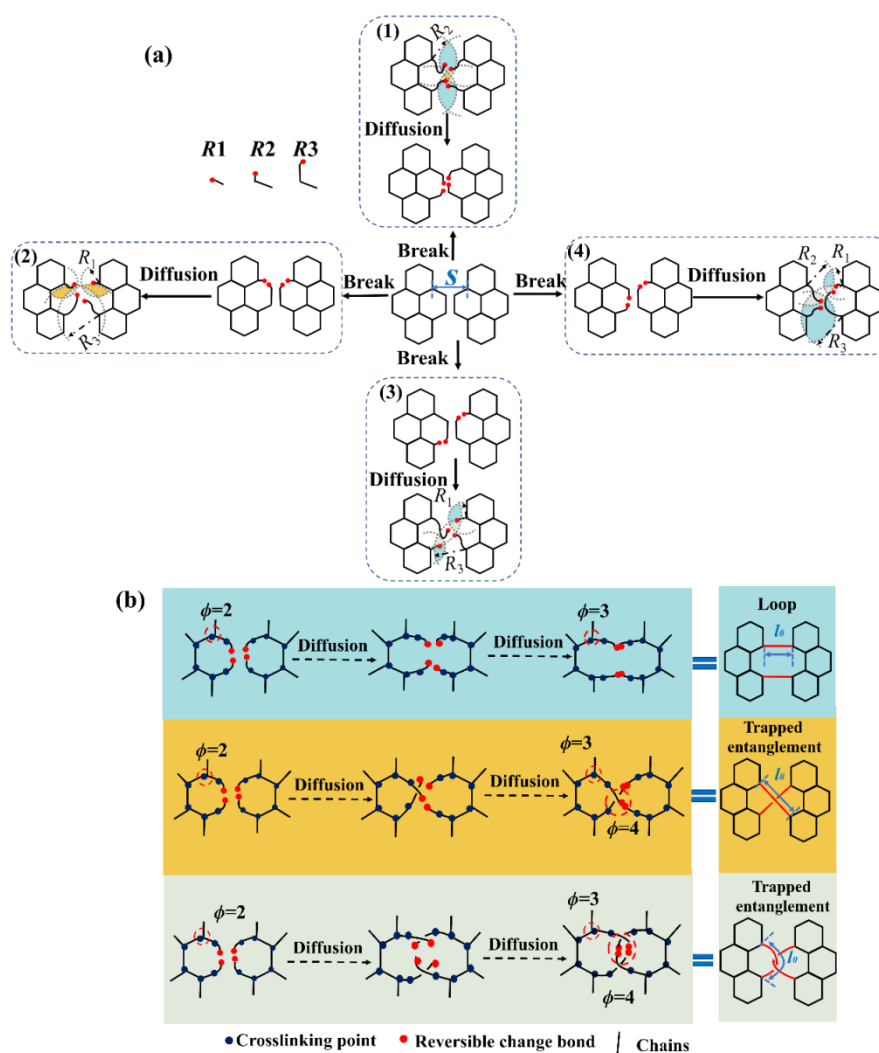
Figure 5. The topological structure of CAN. (a) The chemo-mechano-hydrodynamic coupling effect in CANs. (b) Topological structures of loop and trapped entanglement in CANs.

Figure 5(a) shows that the mechanochemical interactions result in four types of interfacial welding phenomena during the interfacial welding of CANs. A variety of interfacial welding processes have their different elastic free energies, which are

determined by the free-energy equations. According to the phantom network theory,[41] there are three types of topological structures, i.e., one loop structure and two different trapped entanglement structures in the CANs owing to the interfacial welding,[50] as shown in Figure 5(b). R_1, R_2 and R_3 represent the lengths of three types of dangling chains, respectively. l_0 is the diffusion distance of the dangling chains, and S is the interface distance. Here the elastic free energy can be written as:

$$\frac{2\Delta F_{el}}{RT\left(\lambda^2 + 2/\lambda - 3\right)} = \left(1 - \frac{2}{\phi_2}\right)N_2 + \left(1 - \frac{2}{\phi_3}\right)N_3 + \left(1 - \frac{2}{\phi_4}\right)N_4 \tag{6}$$

where N_2 is the molar number of dangling chain, N_3 is the molar number of crosslinking chain, N_4 is the molar number of trapped entanglement chain. $\phi_2 = 2$, $\phi_3 = 3$ and $\phi_4 = 4$ are the functional degrees in the phantom networks for dangling chains, crosslinking chains, and trapped entanglement chains, respectively.

To quantitatively separate the effect of BERs on the elastic free energy of CANs, an assumption was made that there are N_0 of newly formed chains involved in BERs. Therefore, the number of dangling chains is reduced to N_2-$2N_0$, because there are two dangling chains to form a new chain. The number of crosslinking chains is increased to N_3+$2N_0$, because there are $2N_0$ chains involved in the CANs. Meanwhile, the number of trapped entanglement chains is increased to N_4+$\dfrac{N_0}{3}$, because there are three dangling chains to form a trapped entanglement chain. Therefore, equation (6) can be further rewritten for the CANs (after interfacial welding) as follows,

$$\begin{aligned}
&\frac{2\Delta F_{el}}{RT\left(\lambda^2 + 2/\lambda - 3\right)} \\
&= \left(1 - \frac{2}{\phi_2}\right)(N_2 - 2N_0) + \left(1 - \frac{2}{\phi_3}\right)(N_3 + 2N_0) + \left(1 - \frac{2}{\phi_4}\right)(N_4 + \frac{N_0}{3})
\end{aligned} \tag{7}$$

We then employed FEA to study the effects of topological structures of the loop (for interfacial welding) and entanglement (for self-toughening) on the mechanical properties of the CAN. In the FEA, a hexagonal infrastructure with an edge of 10 mm and a thickness of 1 mm was used to describe the entire network structure. A quadratic tetrahedral element, C3D10, was used, and the number of elements was 11000. Boundary conditions were applied to fix constraints on the nodes of one side and uniform displacement loads on the other side, in order to analyze the differences in mechanical properties of the loop and entanglement.
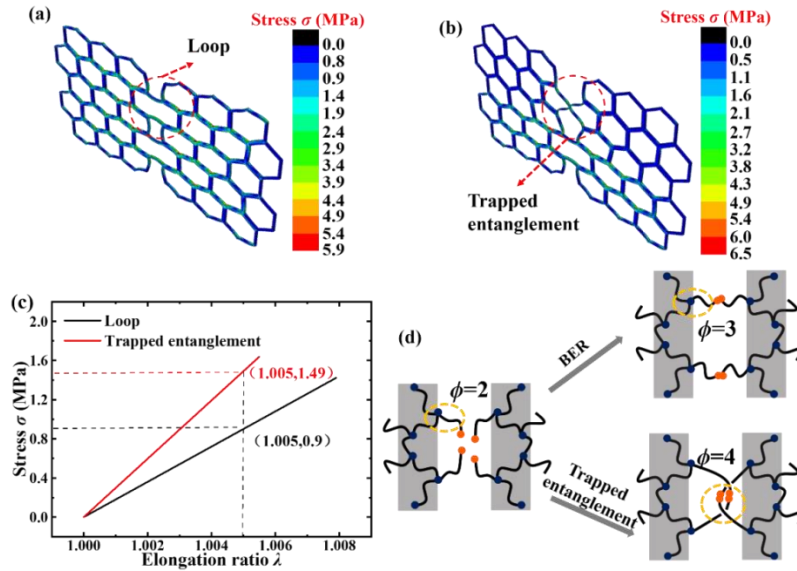
Figure 6. Comparison of mechanical stresses of (a) loop and (b) trapped entanglement topologies. (c) Stress-elongation ratio curves. (d) Illustrations of the functional degrees of CANs undergoing BER and trapped entanglement, respectively.

The obtained simulation results are shown in Figures 6(a) and 6(b), which reveal that the mechanical stresses are 0.90 MPa and 1.49 MPa for the loop and entanglement topology structures, respectively, at the same elongation ratio of 1.005, as shown in Figure 6(c). An increment rate of 166% in the mechanical stress has been presented in comparison of the trapped entanglement structure (the functional degree

ϕ=4) with that of the loop structure (ϕ=3). Therefore, the interfacial welding mechanical stress of loop structure and self-toughening mechanical stress of trapped entanglement structure can be described using the functional degree (ϕ), as illustrated in Figure 6(d).

3.3 Constitutive stress-elongation ratio relationship

Furthermore, the constitutive relationship between stress and elongation ratio has been investigated for the epoxy, which undergoes the BERs and trapped entanglements. Based on the rubber elasticity theory,[28,35] the modulus of epoxy polymer is influenced by the diffusion coefficient of solvent molecules, which is determined by the relaxation time. For the CANs, there are two types of relaxation times, i.e.,

$$\tau_s = \tau_b + \tau_c \tag{8}$$

where τ_b and τ_c represent the BER time and diffusion time, respectively. The chain diffusivity is related to its diffusion distance and diffusion time, e.g., $l_0^2 = D_{coop}\tau_c$.[51]

Based on equation (5), Stukhalin et al. proposed the expression for relaxation time (τ_b) as,[52]

$$\tau_b \approx \tau_0 \exp\left(\frac{E_0}{RT} + \gamma \frac{V_0}{V - k_{so}\Delta Vt - V_0}\right) \tag{9}$$

where τ_0 is the diffusion time for the monomer and E_0 is the energy barrier of BER.

The exchangeable bonds contained in a unit volume of N_0 can be expressed as:

$$N_0 = \frac{N_{01}t}{\tau_s} \tag{10}$$

where N_{01} is number of reaction chains per unit volume.

Combining equations (5), (7), (8), (9) and (10), the constitutive relationship

between stress and elongation ratio under uniaxial tension is obtained:

$$\sigma = \left(\sum_{i=2,3,4} \left(1 - \frac{2}{\phi_i} \right) N_i + \frac{\left(13/6 - 4/\phi_3 - 1/3\phi_4 \right) N_{01} t}{\tau_0 + \frac{l_0^2}{D_{oc}} \exp\left(\frac{E_{as} - E_0}{RT} + \frac{\gamma V_0 / \Delta V}{1 - k_{so} t} + \frac{E_0}{RT} \right)} \right) RT \left(\lambda - \frac{1}{\lambda^2} \right) \quad (11)$$

4. EXPERIMENTAL VERIFICATIONS

To experimentally verify equation (11), the analytical results are plotted to predict

the constitutive stress-elongation ratio relationship of the epoxy polymers with

various soaking times, welding times, and concentrations of catalysts. The obtained

experimental and analytical results are shown in Figure 7. All the parameters used in

equation (11) are listed in Table 1.

Table 1. Parameters used in the model for calculations

	γ	D_{0c} (m^2/s)	E_{as} (J/mol)	E_0 (J/mol)	τ_0 (s)	V (m^3)	V_0 (m^3)	k_{so} (s^{-1})
Value	0.6	9.6×10^{-11}	26.8×10^3	1.22×10^3	0.023	1.61×10^{-9}	1.41×10^{-9}	3.98×10^{-5}
Ref.	34	53	33					

With a catalysts' concentration of 1%, the mechanical stress is increased from 1.12

MPa, 1.26 MPa to 1.48 MPa at the same elongation ratio of 1.001, which is mainly

resulted from the interfacial welding of CANs. With an increase in the welding time

from 45 min (red dots) to 60 min (black dots), the mechanical stress is significantly

increased from 1.26 MPa to 1.48 MPa, resulted from the increase in the interfacial

welding time of CAN in epoxy, as shown in Figure 7(a).

On the other hand, the analytical results obtained from the proposed model based

on equation (11) are close to the experimental results of epoxy polymer undergoing

soaking for 45 min and 60 min, respectively, as revealed in Figure 7(b). Both the

analytical and experimental results reveal that the interfacial welding stress is 0.17 MPa for the epoxy polymer with a soaking time of 45 min, while it is 0.27 MPa with a soaking time of 60 min. Figure 7(c) illustrates the working principles of the effects of catalyst concentration, soaking time and welding time, all of which influence the functional degree (ϕ) and mechanical stress of the epoxy polymer.
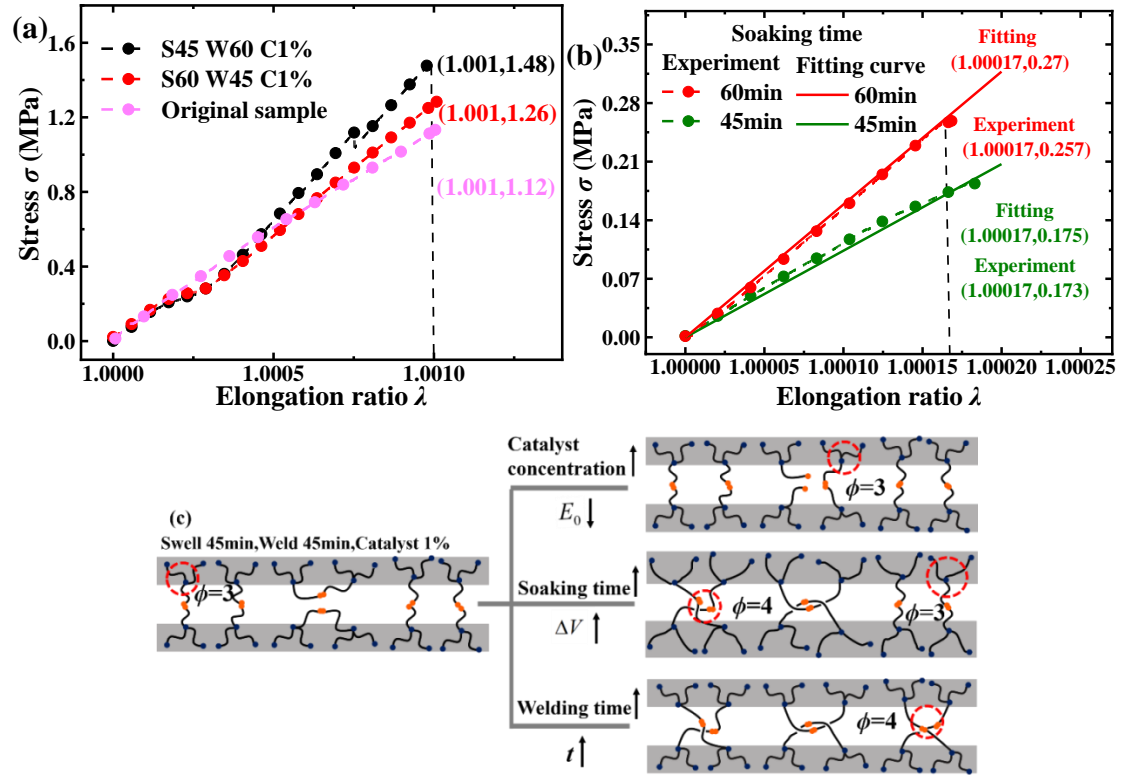
Figure 7. Analytical results from equation (11) and experimental data of mechanical stress-elongation ratio behaviors of epoxy polymers. (a) Interfacial welding of CAN in epoxy with a variety of catalyst concentrations, soaking times and welding times. (b) Analytical results from equation (11) and experimental data of mechanical stress-elongation ratio behaviors of epoxy polymers undergoing soaking times 45 min and 60 min. (c) Schematic illustrations of the effect of functional degree on the phantom networks undergoing interfacial welding.

Furthermore, it is necessary to explore the dependence of functional degree (ϕ) on the topology signatures and their transitions, which are expected to play essential roles to determine the mechanical elasticity of the CANs undergoing a variety of

soaking and welding times[37-40]. The self-healing mechanical behavior of the CANs is incorporated from two parts, i.e., interfacial welding and self-toughening, which can enhance the functional degree (ϕ).

Figure 8 plots the stress values as functions of diffusion distance and time of the dangling chain. The constitutive relationship between the interfacial welding ratio and diffusion distance (l_0) of the epoxy polymer is plotted in Figure 8(a). The obtained analytical results based on equation (11) reveal that the interfacial welding ratio is gradually decreased from 112% to 70% with an increase of diffusion distance (l_0) from 1 nm to 6 nm. In the range of diffusion distance (l_0) from 1 nm to 3 nm, the CANs show both interfacial welding and self-toughening behaviors. However, the CANs only show an interfacial welding behavior, in the diffusion distance (l_0) from 3 nm to 6 nm.
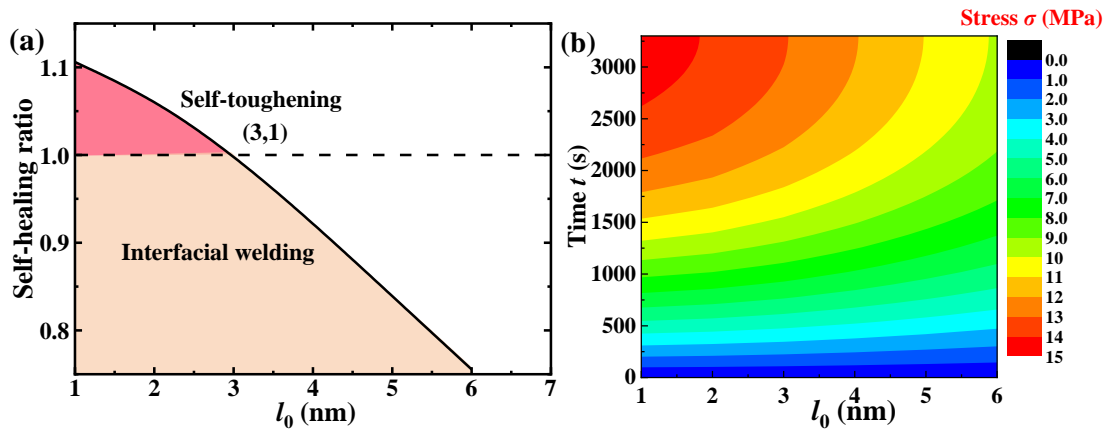
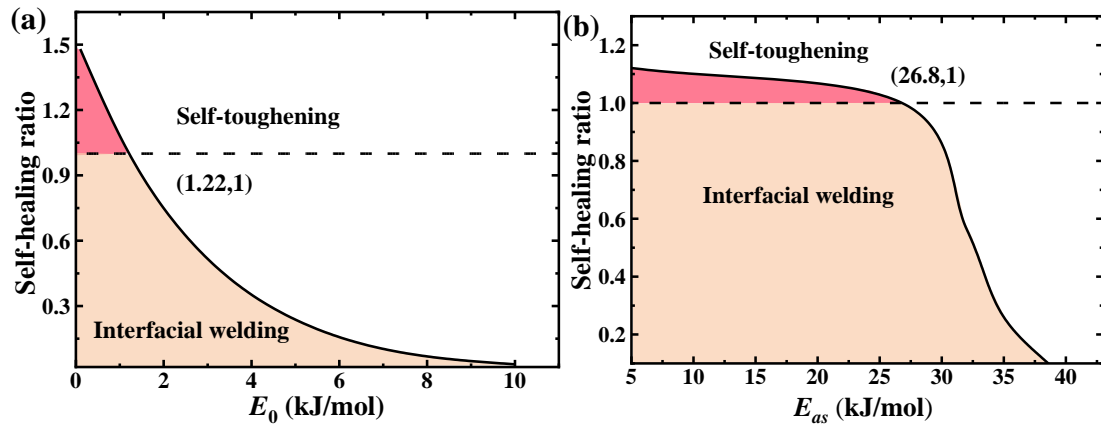**Figure 8**. Effects of diffusion distance and diffusion time on the interfacial welding ratio of the CAN. (a) Interfacial welding ratio as a function of diffusion distance. (b) The contour chart of the stress of CAN as functions of diffusion distance and diffusion time.

Moreover, a cloud chart of stresses as functions of the diffusion distance and diffusion time is shown in Figure 8(b). It is revealed that larger stress of CAN is

resulted from a smaller diffusion distance and higher diffusion time. There is clearly a coupling effect between diffusion distance (l_0) and diffusion time (t) on the interfacial welding mechanical stress (σ) of the CANs.

On the other hand, the effects of the energy barrier of BERs (E_0) and diffusion activation energy (E_{as}) on the interfacial welding ratio have been investigated based on equation (11) and the obtained results are plotted in Figure 9. With an increase in the energy barrier of BERs (E_0) from 0 kJ/mol to 10 kJ/mol, the interfacial welding ratio is gradually decreased from 150% to 0% when the diffusion activation energy (E_{as}) is kept a constant. Within the range of energy barrier of BER (E_0) from 0 kJ/mol to 1.22 kJ/mol, the CANs show both interfacial welding and self-toughening behaviors. Whereas in the range of the energy barrier of BERs (E_0) from 1.22 kJ/mol to 10 kJ/mol, the CANs only show an interfacial welding behavior, as revealed in Figure 9(a).

Figure 9. Effects of energy barrier of BER and diffusion activation energy on interfacial welding ratio of the CAN. (a) Interfacial welding ratio as a function of energy barrier of BER. (b) Interfacial welding ratio as a function of diffusion activation energy.

At a constant energy barrier of BERs (E_0), the diffusion activation energy (E_{as}) plays a critical role to determine the interfacial welding ratio of CANs, as presented in Figure 9(b). With an increase in diffusion activation energy (E_{as}) from 5 kJ/mol to 38 kJ/mol, the interfacial welding ratio is gradually decreased from 115% to 10%. If the range of diffusion activation energy (E_{as}) is changed from 5 kJ/mol to 26.8 kJ/mol, the CAN shows both interfacial welding and self-toughening behaviors. While it only shows an interfacial welding behavior in the range of diffusion activation energy (E_{as}) from 26.8 kJ/mol to 38 kJ/mol.
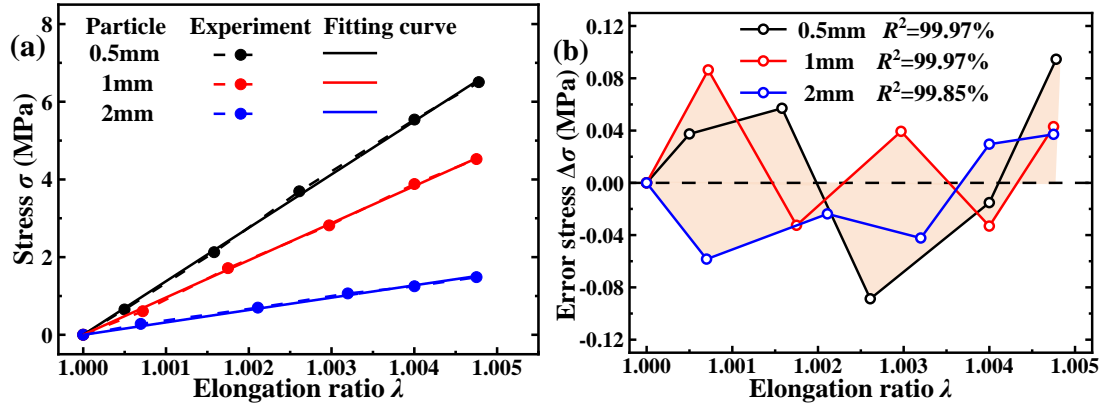
Figure 10. (a) Comparisons of analytical results of equation (11) and experimental data of anhydride-cured epoxy polymer with different particle sizes.[54] (b) Divergences of analytical and experimental results of stress.

Figure 10(a) shows the reported mechanical properties of anhydride-cured epoxy polymer with different particle sizes.[54] By increasing the particle size from 0.5 mm, 1 mm to 2 mm, the relaxation time is gradually increased from 0.002 s, 0.0032 s to 0.010 s. With a smaller size of the particle, higher mechanical stress is therefore achieved. Furthermore, the correlation indexes (R^2) between the analytical and experimental results were calculated based on the data shown in Figure 10(a), and they are 99.97%, 99.97%, and 99.85% for the different particle sizes, as shown in

Figure 10(b). The obtained R^2 data reveals that the analytical results agree well with the experimental ones ($|\Delta\sigma|<0.095$ MPa).

5. CONCLUSION

In this study, a hydro-chemo-mechanical coupling framework is established to investigate the working principles of hydrodynamic diffusion, chemical BERs and mechanical topology entanglement in interfacial welding of CANs in the epoxy polymer. Topological entanglement has been identified as the key driving force for the self-toughening mechanism, while with BER enables the CANs with a self-healing behavior. Furthermore, an extended phantom network model is developed based on the free volume theory and rubber elasticity theory, to formulate the constitutive stress-elongation ratio relationship for the CANs. The hydro-chemo-mechanical coupling effect has been investigated using the functional degree (ϕ) in the CANs, in terms of diffusion coefficient, free volume, catalyst concentration, welding time and activation energy. Finally, the proposed framework is able to predict the mechanical behaviors of thermosetting epoxy polymer undergoing interfacial welding, and verified using both the FEA simulation and experimental results. This newly developed model provides an in-depth insight into the self-toughening mechanism of mechanical topology entanglement, which governs the hydro-chemo-mechanical coupling effect and self-toughening behavior of the CANs in thermosetting epoxy polymer.

Notes

The authors declare no competing financial interest.

REFERENCES

(1) Montarnal, D.; Capelot, M.; Tournilhac, F.; Leibler, L. Silica-like malleable materials from permanent organic networks. *Science* **2011**, *334*, 965-968.

(2) Ying, H. Z.; Zhang, Y. F.; Cheng, J. J. Dynamic urea bond for the design of reversible and self-healing polymers. *Nat. Commun*. **2014**, *5*, 3218.

(3) Denissen, W.; Winne, J. M.; Prez, F. Vitrimers: permanent organic networks with glass-like fluidity. *Chem. Sci*. **2015**, *7*, 30-38.

(4) Yang, M. Y.; Lu, X. L.; Wang, Z. H.; Fei, G. X.; Xia, H. S. A novel self-catalytic cooperative multiple dynamic moiety: towards rigid and tough but more healable polymer networks. *J. Mater. Chem. A* **2021**, *9*, 16759-16768.

(5) Bergman, S. D.; Wudl, F. Mendable polymers. *J. Mater. Chem*. **2008**, *18*, 41-62.

(6) Nishida, H. Development of materials and technologies for control of polymer recycling. *Polym. J*. **2011**, *43*, 435-447.

(7) Pratama, P. A.; Sharifi, M.; Peterson, A. M.; Palmese, G. R. Room temperature self-healing thermoset based on the diels-alder reaction. *ACS Appl. Mater. Inter*. **2013**, *5*, 12425-12431.

(8) Chen, X. X.; Dam, M. A.; Ono, K.; Mal, A.; Shen, H. B.; Nutt, S. R.; Sheran, K.; Wudl, F. A thermally re-mendable cross-linked polymeric material. *Science* **2002**, *295*, 1698-1702.

(9) Schulte, B.; Tsotsalas, M.; Becker, M.; Studer, A.; De Cola, L. Dynamic microcrystal assembly by nitroxide exchange reactions. *Angew. Chem. Int. Ed.* **2010**, *49*, 6881–6884.

(10) Yu, F.; Cao, X. D.; Du, J.; Wang, G.; Chen, X. F. Multifunctional hydrogel with good structure integrity; self-healing and tissue-adhesive property formed by combining Diels–Alder click reaction and acylhydrazone bond. *ACS Appl. Mater. Inter*. **2015**, *7*, 24023–24031.

(11) Xu, Y. R.; Chen, D. J. A novel self-healing polyurethane based on disulfide bonds. *Macromol. Chem. Phys.* **2016**, *217*, 1191–1196.

(12) Memon, H.; Wei, Y. Welding and reprocessing of disulfide-containing thermoset epoxy resin exhibiting behavior reminiscent of a thermoplastic. *J. Appl. Polym. Sci.* **2020**, *137*, e49541.

(13) Zhou, F. T.; Guo, Z. J.; Wang, W. Y.; Lei, X. F.; Zhang, B. L.; Zhang, H. P.; Zhang, Q. Y. Preparation of self-healing, recyclable epoxy resins and low-electrical resistance composites based on double-disulfide bond exchange. *Compos. Sci. Technol.* **2018**, *167*, 79-85.

(14) Garcia, J. M.; Jones, G. O.; Virwani, K.; McCloskey, B. D.; Boday, D. J.; ter Huurne, G. M.; Horn, H. W.; Coady, D. J.; Bintaleb, A. M.; Alabdulrahman, A, M, S.; Alsewailem, F.; Almegren, H. A. A.; Hedrick, J. L. Recyclable, strong thermosets and organogels via paraformaldehyde condensation with diamines. *Science* **2014**, *344*, 732–735.

(15) Craun, G. P.; Kuo, C. Y.; Neag, C. M. Transesterification cure for coatings: Catalysis by epoxy and nucleophiles. *Prog. Org. Coat.* **1996**, *29*, 55–60.

(16) Singh, G.; Sundararaghavan, V. Modeling self-healing behavior of vitrimers using molecular dynamics with dynamic cross-linking capability. *Chem. Phys. Lett.* **2020**, *760*, 137966.

(17) Chabert, E.; Vial, J.; Cauchois, J. P.; Mihaluta, M.; Tournilhac, F. Multiple welding of long fiber epoxy vitrimer composites. *Soft Matter* **2016**, *12*, 4838–4845.

(18) Paolillo, S.; Bose, R. K.; Santana, M. H.; Grande, A. M. Intrinsic self-healing epoxies in polymer matrix composites (PMCs) for aerospace applications. *Polymers-Basel* **2021**, *13*, 201.

(19) Li, Y. H.; Guo, W. J.; Li, W. J.; Liu, X.; Zhu, H.; Zhang, J. P.; Liu, X. J.; Wei, L. H.; Sun, A. L. Tuning hard phase towards synergistic improvement of toughness and self-healing ability of pol (urethane urea) by dual chain extenders and coordinative bonds. *Chem. Eng. J.* **2020**, *393*, 124583.

(20) Chen, Z. Q.; Sun, Y. C.; Wang, J. T.; Qi, H. J.; Wang, T. J.; Naguib, H. E.

Flexible, reconfigurable, and self-healing TPU/vitrimer polymer blend with copolymerization triggered by bond exchange reaction. *ACS Appl. Mater. Int.* **2020**, *12*, 8740-8750.

(21) Funahashi, Y.; Xin, Y. Z.; Kato, K.; Nguyen, H. H.; Shirai, T. Enhanced electrical property of graphite/Al2O3composite fabricated by reductive sintering of gel-casted body using cross-linked epoxy polymer. *J. Adv. Ceram.* **2022**, *11*, 523-531.

(22) Manjunatha, C. M.; Srihari, S. A brief review on the fatigue behavior of continuous fiber reinforced thermosetting epoxy polymer based nanocomposites. *Transactions of the Indian National Academy of Engineering* **2022**, *7*, 501-507.

(23) Rakotondravao, H. M.; Ishizuka, N.; Sakakibara, K.; Wada, R.; Ichihashi, E.; Takahashi, R.; Takai, T.; Horiuchi, J-I.; Kumada, Y. Characterization of a macroporous epoxy-polymer based resin for the ion-exchange chromatography of therapeutic proteins. *J. Chromatogr. A* **2021**, *1656*, 462503.

(24) Zhang, F.; Zhang, L.; Yaseen, M.; Huang, K. A review on the self-healing ability of epoxy polymers. *J. Appl. Polym. Sci.* **2020**, *138*, e50260.

(25) Khan, A.; Ahmed, N.; Rabnawaz, M. Covalent adaptable network and self-healing materials: current trends and future prospects in sustainability. *Polymers-Basel* **2020**, *12*, 2027.

(26) Shi, X. J.; Luo, C. Q.; Lu, H. B.; Yu, K. Primary recycling of anhydride-cured engineering epoxy using alcohol solvent. *Polym. Eng. Sci.* **2019**, *59*, E111-E119.

(27) He, X.; Hanzon, D. W.; Yu, K. Cyclic welding behavior of covalent adaptable network polymers. *J. Polym. Sci. Pol. Phys.* **2017**, *56*, 402-413.

(28) Yang, T.; Wang, C. H.; Zhang, J.; He, S.; Mouritz, A. P. Toughening and self-healing of epoxy matrix laminates using mendable polymer stitching. *Compos. Sci. Technol.* **2012**, *72*, 1396-1401.

(29) Kumar, R.; Sharma, L.; Chhibber, R.; Dixit, A.; Singhal, R. Environmental degradation of glass fiber-reinforced nanocomposites with self-healing reinforcement in polymer matrix for wind turbine blade application. *T. Indian. I. Metals* **2021**, *74*, 3119-3133.

(30) Guo, Y. K.; Han, L.; Zhao, P. X.; Wang, X. F.; Astruc, D.; Shuai, M. B. Thermo-

reversible MWCNTs/epoxy polymer for use in self-healing and recyclable epoxy adhesive. *Chinese J. Polym. Sci.* **2017**, *35*, 728-738.

(31) Ghazali, H.; Ye, L.; Amir, A. N. Microencapsulated healing agents for an elevated-temperature cured epoxy: influence of viscosity on healing efficiency. *Polym. Polym. Compos.* **2021**, *29*, S1317-S1327.

(32) Yu, K.; Shi, Q.; Li, H.; Jabour, J.; Yang, H.; Dunn, M. L.; Wang, T. J.; Qi, H. J. Interfacial welding of dynamic covalent network polymers. *J. Mech. Phys. Solids* **2016**, *94*, 1-17.

(33) Shi, X. J.; Luo, C. Q.; Lu, H. B.; Yu, K. Interfacial welding and reprocessing of engineering thermosets based on surface depolymerization. *Surf. Interfaces* **2021**, *26*, 101368.

(34) Macedo, P. B.; Litovitz, T. A. On the relative roles of free volume and activation energy in the viscosity of liquids. *J. Chem. Phys.* **1965**, *42*, 245-256.

(35) Cassagnau, P.; De Loor, A.; Fulchiron, R.; Michel, A. Application of the rubber elasticity theory to the co-crosslinking of ethylene vinyl acetate and ethylene methyl acrylate copolymers by transesterification. *Polymer* **1993**, *34*, 1975-1978.

(36) Zettl, U.; Hoffmann, S. T.; Koberling, F.; Krausch, G.; Enderlein, J.; Harnau, L.; Ballauff, M. Self-diffusion and cooperative diffusion in semidilute polymer solutions as measured by fluorescence correlation spectroscopy. *Macromolecules* **2010**, *42*, 9537-9547.

(37) Shi, X. J.; Ge, Q.; Lu, H. B.; Yu, K. The nonequilibrium behaviors of covalent adaptable network polymers during the topology transition. *Soft Matter* **2021**, *17*, 2104-2119.

(38) Xing, Z. Y.; Lu, H. B.; Fu, Y. Q. Anchoring-mediated topology signature of self-assembled elastomers undergoing mechanochromic coupling/decoupling. *Soft Matter* **2021**, *17*, 5960-5968.

(39) Xing, Z. Y.; Li, Z. H.; Lu, H. B.; Fu, Y. Q. Self-assembled topological transition via intra- and inter-chain coupled binding physical hydrogel towards mechanical toughening. *Polymer* **2021**, *235*, 124268.

(40) Zhong, M. J.; Wang, R.; Kawamoto, K.; Olsen, B. D.; Johnson, J. A. Quantifying

the impact of molecular defects on polymer network elasticity. *Science* **2016**, *35*, 1264-1268.

(41) Treloar, L. R. G. *The physics of rubber elasticity*; Oxford Uni. Press: New York, 1975.

(42) Chen, M.; Zhou, L.; Chen, Z. T.; Zhang, Y. Y.; Xiao, P. S.; Yu, S. J.; Wu, Y, P.; Zhao, X. L. Multi-functional epoxy vitrimers: Controllable dynamic properties; multiple-stimuli response; crack-healing and fracture-welding. *Compos. Sci. Technol.* **2022**, *221*, 109364.

(43) An, L.; Zhao, W. Z. Facile surface depolymerization promotes the welding of hard epoxy vitrimer. *Materials* **2022**, *15*, 4488.

(44) Lv, Z. T.; Yang, H. K.; Wang, D. Catalyst control of interfacial welding mechanical properties of vitrimers. *Chinese J. Polym. Sci.* **2022**, *40*, 611-617.

(45) Sun, Y. G.; Yang, H.; Yu, K.; Guo, Y. F.; Qu, J. M. A molecular dynamics study of decomposition of covalent adaptable networks in organic solvent. *Polymer* **2019**, *180*, 121702.

(46) Shi, Q.; Yu, K.; Dunn, M. L.; Wang, T. J.; Qi, H. J. Solvent assisted pressure-free surface welding and reprocessing of malleable epoxy polymers. *Surf. Interfaces* **2019**, *49*, 5527-5537.

(47) Flory, P. J. *Principles of Polymer Chemistry*; Cornell Uni. Press: New York, 1953.

(48) de Gennes, P. G. *Scaling Concepts in Polymer Physics*; Cornell Uni. Press: New York, 1979.

(49) Stukalin, E. B.; Cai, L. H.; Kumar, N. A.; Leibler, L.; Rubinstein, M. Self-healing of unentangled polymer networks with reversible bonds. *Macromolecules* **2013**, *46*, 7525-7541.

(50) Li, C. H.; Wang, Z. J.; Wang, Y.; He, Q. G.; Long, R.; Cai, S. Effects of network structures on the fracture of hydrogel. *Extreme Mech. Lett.* **2021**, *49*, 101495

(51) An, L.; Shi, Q.; Jin, C.; Zhao, W. Z.; Wang, T. J. Chain diffusion based framework for modeling the welding of vitrimers. *J. Mech. Phys. Solids* **2022**, *164*, 104883.

(52) Yu, K.; Yang, H.; Dao, B. H.; Shi, Q.; Yakacki, C. M. Dissolution of covalent

adaptable network polymers in organic solvent. *J. Mech. Phys. Solids* **2017**, *109*, 78-94.

(53) Chen, S. H.; Chu, B.; Nossal, R. *Scattering Techniques Applied to Supramolecular and Nonequilibrium Systems*; Plenum. Press: New York, 1981.

(54) Zhang, B.; Li, H. G.; Yuan, C.; Dunn, M. L.; Qi, H. J.; Yu, K.; Shi, Q.; Ge, Q. Influences of processing conditions on mechanical properties of recycled epoxy-anhydride vitrimers. *J. Appl. Polym. Sci.* **2020**, *137*, e49246.